Metrologically traceable quantification of trifluoroacetic acid content in peptide reference materials by ^{19}F solid-state NMR

Brinkmann, Andreas; Raza, Mohammad; Melanson, Jeremy E.

Publisher's version / Version de l'éditeur:
https://doi.org/10.1088/1681-7575/ab04e3
Metrologia, 56, 2, pp. 1-10, 2019-02-22

Metrologically traceable quantification of trifluoroacetic acid content in peptide reference materials by ^{19}F solid-state NMR

Andreas Brinkmann*, Mohammad Raza‡, and Jeremy E. Melanson

Metrology, National Research Council Canada, 1200 Montreal Road, Ottawa, ON K1A 0R6, Canada

E-mail: Andreas.Brinkmann@nrc-cnrc.gc.ca

Abstract. Although solution-state NMR is frequently used in metrologically-traceable quantification studies, this is not the case for solid-state NMR. However, solid-state NMR allows quantification of substances without the need of dissolution, providing a truly non-destructive approach, and extending metrologically-traceable quantitative NMR to sample classes that are difficult to characterize in solution. In this contribution we present a thorough and rigorous protocol for ^{19}F quantitative solid-state NMR employing a certified reference material as external calibrant to provide metrological traceability to absolutely quantify the content of trifluoroacetic acid (TFA) in a peptide sample, typically the major impurity in synthetic peptides. The protocol includes determining the quantitative volume of the solid-state NMR sample holder (rotor), the ERETIC (Electronic REference To access In vivo Concentrations) method [Akoka *et al.* 1999 *Anal. Chem.* **71** 2554] to compensate for variations in the sensitivity of the radio frequency resonant circuit when an external calibrant is used, and the EASY (Elimination of Artifacts in NMR Spectroscopy) method [Jaeger & Hemmann 2014 *Solid State Nucl. Magn. Reson.* **57–58** 22] to effectively suppress the ^{19}F NMR background signal from the probehead. We applied the protocol to quantify the amount of TFA in a candidate NRC certified reference material of the peptide angiotensin II. The results obtained by ^{19}F quantitative solid-state NMR are in excellent agreement with those obtained by quantitative NMR in solution employing an internal calibrant.

Keywords: quantitative solid-state NMR, ^{19}F NMR, qNMR, traceability, TFA, peptides

Submitted to: *Metrologia*, Special Issue *Focus on Advances in Metrology in Chemistry and Biology*

‡ Present address: Department of Chemistry & Chemical Biology, and Brockhouse Institute for Materials Research, McMaster University, 1280 Main St. West, Hamilton ON L8S 4M1, Canada

1. Introduction

Peptides are chains of amino acids linked by amide bonds, ranging in length of only a few amino acids up to roughly 50 amino acids, beyond which they are generally considered proteins. The accurate measurement of peptides is crucial for many clinical diagnostic assays [1], and also in the development and manufacturing of peptide-based therapeutics. Therefore, the availability of well-characterized peptide reference materials are vital for these sectors.

Relative to small molecules, peptides are typically more difficult to obtain at high purity. Generally prepared by solid phase peptide synthesis (SPPS), impurities can result from the insertion of incorrect amino acids, with specific sequences being more prone to this affect [2]. In addition, strong acids such as trifluoroacetic acid (TFA) are used to cleave the peptide from the solid support and to remove all protecting groups, which can then co-crystallize with the peptide [2]. Depending on the number of basic sites of the peptide, large amounts of TFA counter-ion can results, in some cases up to 25 % by weight [3]. If determining peptide purity by conventional means, such as by LC-UV, the amount of these salts can be greatly underestimated or completely undetected [2], thereby significantly over-estimating the peptide purity level.

For more accurate peptide purity measurements, specific methods to detect peptide counter-ions such as TFA would be valuable. Accurate determination of TFA levels in a peptide reference material has been demonstrated using ^{19}F quantitative nuclear magnetic resonance spectroscopy (^{19}F-qNMR) in solution using an internal calibrant [3]. This approach has been successfully validated against ion chromatography methods in an international comparison exercise [4]. Despite the high performance of this method, it requires a relatively large amount of peptide sample per analysis (typically 1 to 10 mg) [3], which generally cannot be recycled once in deuterated solvent containing the calibrant. This sample requirement is particularly detrimental when a large number of related peptide impurities are acquired that need purity assigned prior to use as quantitative standards for measuring these impurities by mass spectrometry in a peptide reference material [5–7]. The cost of these custom synthesized peptides can be very high, especially in the case of isotopically labelled peptides, even for quantities such as 10 mg. Therefore, a non-destructive method to measure TFA that would allow for the entire sample to be re-used for quantitative analysis would offer significant advantages.

Switching from an internal calibrant to an external one provides a partial solution to this problem, although retrieval from the deuterated solvent may still be difficult or impossible. In addition, the use of an external calibrant prevents possible chemical interactions between calibrant and analyte molecules in the sample. However, the use of an external calibrant in qNMR requires to correct for changes in the quality factor

(Q factor) of the radio frequency (rf) resonance circuit containing the rf coil used for excitation and detection of the NMR signal. These differences in the Q factor alter the sensitivity of the NMR signal detection between sample changes. Two methods have been developed to correct qNMR experiments employing external calibrants in this event: (i) In the ERETIC (Electronic REference To access In vivo Concentrations) method [8–11] an artificial electronic signal is injected into a separate rf circuit of the NMR probehead and observed together with the NMR signal during the detection period of the experiment. (ii) In the PULCON (pulse length based concentration determination) method [12] the NMR signal intensities obtained in separate measurements on the calibrant and analyte are corrected by the rf field strength generated in the rf coil (usually determined by measuring the 360° pulse duration), as according to the reciprocity principle [13] the rf circuit's sensitivity in detecting the NMR signal is proportional to the rf field strength generated.

Ultimately, the only true non-destructive approach to qNMR is to quantify the analyte in the solid state. Although solution-state NMR is frequently used in quantification studies [14,15], this is less true for solid-state NMR [16,17]. In order to increase the sensitivity and resolution of solid-state NMR spectra, *magic-angle spinning* (MAS) [18, 19] is employed, in which the sample is rapidly rotated about an axis at the "magic angle" of 54.74°, with respect to the static magnetic field in order to average anisotropic spin interactions that lead to broadening of the resonance lines. Especially, ^{13}C cross-polarization magic-angle-spinning (CP-MAS) NMR [20,21] has been successfully employed to quantify polymorhps of organic molecules and formulations of pharmaceutical active ingredients [17, 22–29]. As the efficiency of cross polarization is dependent on the molecular and crystal structure of the sample, ^{13}C CP-MAS NMR only allows on one hand to quantify different chemical groups or polymorphs within the same sample *relative* to each other, especially if multiple-contact CP (MC-CP) is employed [30–36]. Relative quantification by ^{13}C CP-MAS NMR has also been used to determine the crystallinity index, polymorphism and specific surface area in cellulose samples [37–56]. On the other hand, absolute quantification of the unknown amount of a certain analyte molecule in a sample is enabled, if the *identical* molecule is also used as a calibrant, i. e. if a calibration curve is obtained correlating the CP signal intensity to the calibrant concentration in a series of mixtures prepared with a known calibrant concentration [23, 27, 57, 58]. Care must be taken though that the mixtures prepared for calibration possess similar physical and chemical properties as the target material. However, strictly, this approach also requires compensation by PULCON or ERETIC, as discussed above, due to variations in the rf circuit's sensitivity when the NMR samples are changed, although to our knowledge this has not be done at this point.

The use of direct polarization is highly favourable for solid-state qNMR as the integrated NMR signal intensity is directly proportional to the number of nuclei contributing to the NMR resonance. Furthermore, choosing a nucleus possessing both

high natural abundance and high gyromagnetic ratio assures that a sufficient signal to noise ratio can easily be obtained for accurate quantification. Unfortunately, the obvious choice in the solution state, ^{1}H-qNMR, is not an easy task in the solid state because of the small proton chemical shift range and the network of strong homonuclear ^{1}H dipolar couplings, resulting in broad overlapping resonances, even under magic-angle-spinning conditions [59]. However, ^{19}F magic-angle-spinning solid-state NMR has emerged as powerful method for quantification studies, as it combines the advantage of the high sensitivity of ^{19}F nuclei due to their high gyromagnetic ratio with high selectivity, i. e. the ^{19}F NMR signals of the fluorinated probe molecules are inherently separated from the often overwhelming proton NMR signal stemming from the bulk material.

Recently, ^{19}F magic-angle-spinning solid-state NMR provided conclusive evidence for the occurrence of elemental F_2 in some varieties of the mineral fluorite. Furthermore, the use of an internal calibrant allowed to quantify the F_2 content [60]. ^{19}F solid-state qNMR employing external calibrants has been used to study the degradation of Nafion fuel cell membranes [61], to quantify accessible hydroxyl sites on fiberglass surfaces [62], to quantify organo fluorines absorbed on inorganic surfaces [63, 64], to determine the reactive surface area of clay minerals [65], to quantify the amount of surface functional groups of coumarin-stained beads [66], and to determine the fluorine content in 2,2,2-trifluoroethylamine labeled polymer particles [67]. In the latter case, metrological traceability was achieved by using a certified reference material (CRM) as external calibrant. However, so far solid-state ^{19}F-qNMR using an external calibrant has not been combined with either PULCON or ERETIC to correct for changes in the Q factor of the probehead under sample changes.

In this contribution we present a thorough and rigorous protocol for ^{19}F solid-state qNMR employing a CRM as external calibrant to provide metrological traceability to absolutely quantify the content of TFA in as-synthesized peptide samples. The protocol includes (i) determining the quantitative volume of the solid-state NMR sample holder (rotor), (ii) employing the ERETIC method [8–11] to compensate for variations in the sensitivity of the radio frequency resonant circuit in the NMR probehead when an external calibrant is used, and (iii) using the EASY (Elimination of Artifacts in NMR Spectroscopy) method [68, 69] to effectively suppress the ^{19}F NMR background signal from the NMR probehead. We applied the protocol to quantify the amount of TFA in a sample of the peptide angiotensin II candidate NRC certified reference material ANGII-1.

2. Materials and methods

2.1. Materials

The powdered samples of the peptide angiotensin II (analyte) were taken from a unit of the candidate NRC CRM ANGII-1, and used without any further purification. In order to quantify the ^{19}F solid-state NMR experiments the external calibrant 3,5-Bis(trifluoromethyl)benzoic acid (BTFMBA) was chosen and obtained as CRM from the National Metrology Institute of Japan (NMIJ).

2.2. Solid-state NMR spectroscopy

All solid-state experiments were performed at an external magnetic field of 4.6 T (corresponding to 200 MHz proton Larmor frequency) on a Bruker Avance spectrometer console utilizing a commercial Bruker 3.2 mm double-resonance probehead with one $^{1}H/^{19}F$ channel and one broadband X channel. The sample rotation angle with respect to the external magnetic field was set to the magic angle of 54.74° by maximizing the number of rotational echoes in the ^{79}Br free induction decay (FID) in a sample of KBr rotating at a frequency of 3.5 kHz [70]. Excellent shimming of the external magnetic field was verified by obtaining a proton-decoupled ^{13}C spectrum of adamantane at 3.5 kHz magic-angle-spinning frequency. The full width at half maximum (FWHM) of the methylene ^{13}C signal was given by 1.5 Hz. The isotropic chemical shift of the methylene signal was set to 37.77 ppm, acting as a secondary reference to 1 % TMS in $CDCl_3$. Other nuclei were subsequently referenced via the unified chemical shift scale [71].

The ^{19}F experiments were performed at a sample spinning frequency of 18 kHz and the two rf channels of the probehead were tuned to the Larmor frequencies of ^{19}F and ^{13}C, given by 188.7 MHz and 50.4 MHz, respectively. We implemented the ERETIC method [8–11] as shown in figure 1 to enable ^{19}F-qNMR employing an external calibrant to determine the absolute amount of analyte. The ^{19}F ERETIC signal generated by the synthesizer is fed without further amplification into the probe's X channel via a directional coupler [25]. We used a exponentially decaying ERETIC signal with a decay time constant of 1.06 ms, which corresponds to a Lorentzian lineshape with a FWHW of 300 Hz in the NMR spectrum after Fourier transformation. In order to reduce the probehead's ^{19}F background NMR signal, the Teflon sleeve encasing the MAS stator was removed. Furthermore, we employed the EASY method by Jaeger and Hemmann [68, 69] to mostly suppress any remaining ^{19}F NMR signal stemming from the probehead.

As rotating solid-state NMR sample holders we used Bruker zirconia rotors with outer and inner diameters of 3.2 and 2.2 mm ("thick-wall"), respectively, and a length of 15.4 mm. The rotors are sealed by Vespel drive tips, as shown in figure 2. The profile of

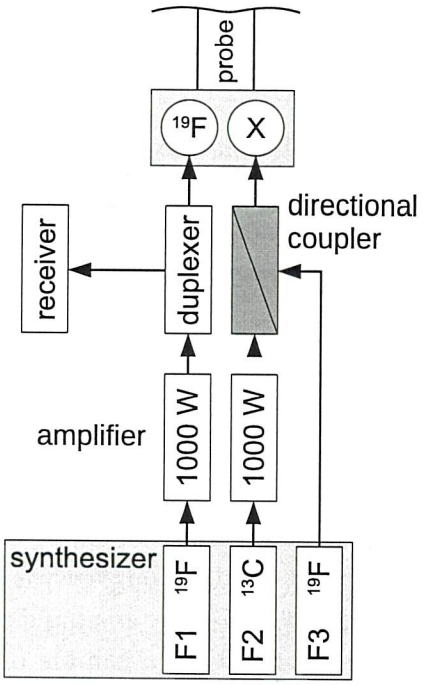

Figure 1. Schematic drawing of the ERETIC setup used in this work: ^{19}F rf pulses are generated by an rf synthesizer and amplified by a high-power amplifier and delivered into the ^{19}F channel of the solid-state NMR probehead. A duplexer allows the detection of the weak NMR signal in the receiver. The artificial ^{19}F ERETIC signal is generated by a separate rf synthesizer and injected into the X channel of the probehead via a directional coupler.

the oscillating rf field B_1 inside the rotor was determined by obtaining the integrated ^{19}F signal intensity of a 1 mm Kel-F (PCTFE, polychlorotrifluoroethylene) disk as a function of its position inside the rotor following the approach of Caldarelli *et al.* [25, 26]. The position of the Kel-F disk was varied by a set of bottom and top spacers made from Delrin (polyoxymethylene) with varying heights. The different parts of the solid-state NMR rotor together with the spacers are shown in figure 2 and the heights of the bottom and top spacers are listed in table 1.

The mass of the angiotensin II and BTFMBA samples were determined gravimetrically using a Mettler XP-6U balance by subtracting the mass of the plain rotor assembly (rotor, drive tip and spacers) from the mass of the rotor assembly filled with the respective sample. The balance was exercised and calibrated prior to each weighing. It was kept in a constant temperature and humidity environment (21° C and 47 %).

Prior to performing the ^{19}F-qNMR experiments employing both ERETIC and EASY, the ^{19}F spin-lattice relaxation time T_1 in both the calibrant and analyte was determined

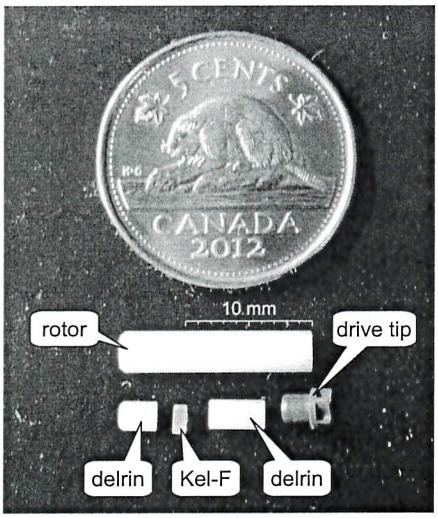

Figure 2. Bruker 3.2 mm zirconia solid-state NMR rotor together with Vespel drive tip, Delrin and Kel-F inserts.

with the help of a saturation recovery experiment [72]. We determined the ^{19}F T_1 to be 2.87 s and 1.81 s for BTFMBA and TFA in the angiotensin II sample, respectively. Subsequently, a recovery or relaxation delay of $7 \times T_1$ was used in the qNMR experiments, i. e. 20.09 s and 12.64 s for BTFMBA and angiotensin II, respectively. Before each ^{19}F-qNMR experiment the ^{19}F 90° pulse length was determined, typically to be 2.3–2.4 μs. The spectral width was set to 100 kHz, 1024 complex data points were recorded in the time domain, and a total of 2048 transient were co-added. The receiver gain was set identical in all experiments.

2.3. NMR signal processing

The recorded ^{19}F FID data was zero-filled to 4× its original size and subjected to a complex Fourier transformation followed by manually adjusting the spectral phase to zeroth and first order to obtain pure absorption lineshapes. The baseline around the centerband at the isotropic chemical shift and the ±1 and ±2 spinning sidebands was manually corrected using a polynomial. The resulting spectral lines were integrated by summation.

3. Results and Discussion

3.1. Experimental Considerations

In order to fully exploit the benefits of solid-state ^{19}F-qNMR, the experimental solid-state NMR conditions need to be carefully chosen: The ^{19}F chemical shift anisotropy (CSA) of

fluorine nuclei in CF_3, CF_2 and CF functional groups are in the order of 70-90 ppm [73]. Sample rotation at spinning frequencies smaller than the CSA, results in NMR spectra that contain a set of spinning sidebands, separated by the spinning frequency and centered at the isotropic chemical shift [74]. Quantification of the intensity of a particular ^{19}F resonance requires to integrate the complete set of spinning sidebands belonging to that resonance line. Hence, it is beneficial to weigh up the choice of the external magnetic field size against the sample spinning frequencies achievable for a certain sample holder size, in order to achieve ^{19}F magic-angle-spinning solid-state NMR spectra that are almost free of spinning sidebands to facilitate quantification. For example, a CSA of 90 ppm corresponds to frequency values of about 17 kHz and 34 kHz at external magnetic fields of 4.7 and 9.4 T, respectively, where the former corresponds to a proton Larmor frequency of 200 MHz and the latter 400 MHz. Hence, sample spinning with frequencies larger than 17 kHz and 34 kHz is required to achieve ^{19}F spectra almost free of spinning sidebands at 4.7 and 9.4 T, respectively, where the former can be easily achieved with a commercial 3.2 mm sample holder (rotor) and the latter would require a 2.5 mm rotor with significantly less sample volume. Hence, in the case of solid-state ^{19}F-qNMR the non-intuitive choice of a *lower* external magnetic field may be preferable.

As solely the use of an external calibrant enables non-destructive solid-state qNMR that allows sample recovery, either ERETIC or PULCON have to be used to compensate for variations in the sensitivity of the rf circuit when the NMR sample is changed. On the one hand ERETIC requires additional hardware setup, making PULCON an experimentally simpler technique. On the other hand as the solid-state ^{19}F NMR lineshapes are significantly broader than in solution state, and the homogeneity of the rf field in a solenoid coil is larger than in a saddle coil, PULCON is more difficult to use as accurately in solid-state NMR as in solution NMR. Hence, we opted to implement ERETIC as described in detail in section 2.2. At this point we also would like to add, that recently, Bruker has introduced PULCON into their spectrometer processing software, unfortunately referring to it as „ERETIC2", as they enable to add a solely computer generated mathematical reference peak to the NMR spectrum [75]. However, this should not be confused with the genuine ERETIC that relies on a true electronic signal generated by an rf synthesizer and detected in the NMR coil.

Standard solid-state NMR probeheads show strong ^{19}F background signals, mainly from parts containing Teflon. As these parts are abundant and located outside the coil and NMR rotor, the resulting strong resonance lines are very broad, making the accurate quantification of weak calibrant and analyte signals extremely difficult. However, many experimental techniques have been proposed, a review and relevant literature references can be found in Ref. 68. We chose the EASY method recently introduced by Jaeger and Hemmann [68,69] as it is compatible with qNMR in general, because solely a single pulse is

Table 1. Normalized integrated ^{19}F NMR signal intensity I of a 1 mm Kel-F disk as a function of the configuration of the spacers in the 3.2 mm Bruker solid-state NMR rotor: h_b and h_t indicate the height of the bottom and top spacers, respectively.

Configuration	A	B	C	D	E	F
h_b (mm)	1.00	2.00	3.00	4.00	5.00	6.00
h_t (mm)	6.45	5.45	4.45	3.45	2.45	1.45
I (%)	96.65	100.0	97.91	92.47	81.57	53.86

employed and no formation of a spin echo is required. After the relaxation delay (typically $7 \times T_1$ for qNMR applications, where T_1 is the spin-lattice relaxation time), the spin system has returned to thermal equilibrium. During EASY, two FIDs are acquired consecutively without intervening delay, each subsequent to a single 90° pulse. The first FID contains the NMR signal from both the sample inside the rotor and the probe background. The second FID solely contains the background signal. Hence, if the second FID is subtracted from the first, a background-free NMR spectram can be retrieved [68, 69].

3.2. Determination of the Quantitative Volume

Unlike in solution NMR where only part of the sample is located within the rf saddle coil, in MAS solid-state NMR the rotor is placed within an rf solenoid coil. However, the amplitude of the oscillating magnetic field B_1 is highest in the center of the coil and falls off towards both ends of the coil. Hence, although the whole sample experiences the B_1 field, the field is by no means homogeneous over the sample volume. As a result of the reciprocity principle [13] the NMR signal per volume detected by the coil is not constant over the entire sample volume. Thus, in order to employ solid-state NMR to quantify the amount of an analyte in the rotor with the help of an external calibrant, one would need to ensure that the solid samples, often in powder form, are very homogeneously distributed over the sample volume. As this is difficult to achieve in practice a better approach is to determine the volume slice, referred to as the *quantitative volume*, in the rotor over which the NMR response is essentially constant. This would straightforwardly enable qNMR using an external calibrant. It should be noted that the absolute amount of analyte can be determined in this case, not just the concentration as in solution NMR.

In order to determine the quantitative volume we followed the approach of Caldarelli *et al.* [25,26], which we adapted to ^{19}F solid-state NMR: The integrated ^{19}F signal intensity of a 1 mm Kel-F (PCTFE, polychlorotrifluoroethylene) disk was determined as a function of its position inside the rotor, where the positioning of the disk was achieved by a set of bottom and top spacers made from Delrin (polyoxymethylene) with varying heights,

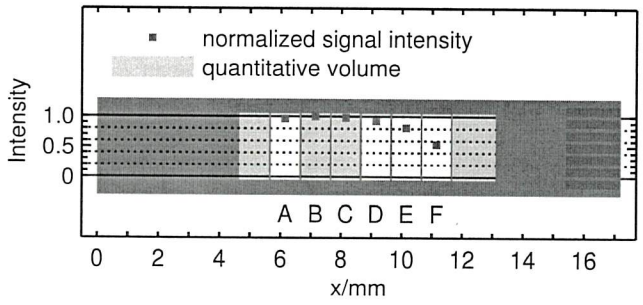

Figure 3. Normalized integrated ^{19}F NMR signal intensity of a 1 mm disk of Kel-F as a function of the position of the disk in the 3.2 mm Bruker solid-state NMR rotor. Indicated in green is the *quantitative volume*, for which the intensity is between 97.9 and 100 %.

as shown in figure 2 and listed in table 1. The integrated ^{19}F signal intensities I were normalized to the maximum value found for configuration B and the results are given in table 1 in %. They are plotted as a function of the position of the Kel-F disk in figure 3.

We note that configurations A, B, C and D show integrated signal intensities larger than 90 %, and slices A, B, and C result in intensities larger than 95 %. Finally, if we solely consider configurations B and C, signal intensities of larger than or equal to 97.9 % can be observed. We choose to call this the quantitative volume of this type of rotor in the specific rf coil used in this particular probhead. With a sample height of 2 mm, the quantitative volume is given by 7.6 μl. It should be noted that this determination of the quantitative volume would need to be executed for each individual probehead as coil configurations might differ.

3.3. Quantitative ^{19}F Solid-State NMR

The top of figure 4 shows typical ^{19}F solid-state NMR spectrum of the analyte trifluoroacetic acid (TFA) in the NRC CRM sample ANGII-1 of the peptide angiotensin II, whereas the bottom of figure 4 depicts a spectrum of the calibrant 3,5-Bis(trifluoromethyl)benzoic acid (BTFMBA). Both spectra show the strong centerband resonance lines stemming from the CF_3 groups at -75.8 ppm and -63.9 ppm for TFA and BTFMBA, respectively. Also note the presence of weak spinning sidebands, separated by the spinning frequency, marked with an asterisk that need to considered when integrating signal intensities. Furthermore, the artificial ERETIC signal is indicated in both spectra.

The mass fraction (purity) w_{ana} of the analyte TFA is determined with the help of the

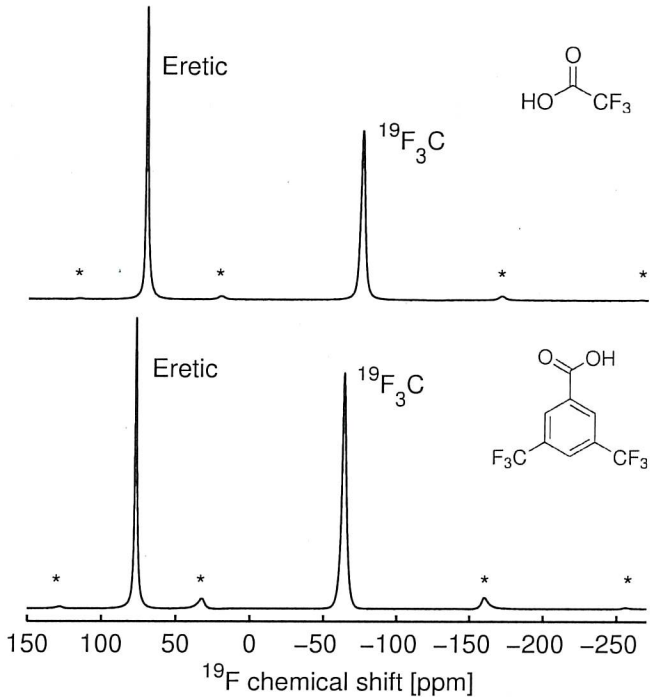

Figure 4. ^{19}F magic-angle spinning solid-state NMR spectra of TFA in angiotensin II (top) and BTFMBA (bottom). Indicated are the resonance lines from the $^{19}F_3C$ groups and the artificial ERETIC signal detected in the NMR coil. Marked with an asterisk are the spinning sidebands.

equation

$$
\begin{aligned}
w_{\text{ana}} &= \frac{I_{\text{ana}}}{I_{\text{cal}}}\frac{I^E_{\text{cal}}}{I^E_{\text{ana}}}\frac{P_{\text{cal}}}{P_{\text{ana}}}\frac{w_{\text{cal}}m_{\text{cal}}}{M_{\text{cal}}}\frac{M_{\text{ana}}}{m_{\text{ana}}} \\
&= \underbrace{\left(\frac{I_{\text{ana}}}{I^E_{\text{ana}}P_{\text{ana}}}\frac{M_{\text{ana}}}{m_{\text{ana}}}\right)}_{I^{\text{norm}}_{\text{ana}}} \times \underbrace{\left(\frac{I_{\text{cal}}}{I^E_{\text{cal}}P_{\text{cal}}}\frac{M_{\text{cal}}}{w_{\text{cal}}m_{\text{cal}}}\right)^{-1}}_{I^{\text{norm}}_{\text{cal}}} \\
&= I^{\text{norm}}_{\text{ana}}/I^{\text{norm}}_{\text{cal}},
\end{aligned}
\tag{1}
$$

where the subscripts "cal" and "ana" refer to the calibrant and analyte, respectively. The symbols m and M indicate the mass and molar mass, respectively. P is the number of nulcei contributing to a particular NMR resonance line. I and I^E are the integrated intensities of the NMR resonance line and the artificial ERETIC signal, respectively. Finally, w_{cal} is the mass fraction (purity) of the calibrant. In the second line of Equation (1) we separated the quantities linked to the analyte and calibrant and defined normalized molar signal intensities $I^{\text{norm}}_{\text{ana}}$ and $I^{\text{norm}}_{\text{cal}}$, respectively. For example, $I^{\text{norm}}_{\text{cal}}$ refers to the ERETIC

Table 2. Integrated experimental ^{19}F NMR signal intensities for a series of trials for a set of BTFMBA (calibrant) samples.

Sample #	m_{cal} (mg)	h_b (mm)	h_t (mm)	quant. volume	Trial #	I^E_{cal} (10^9)	I_{cal} (10^9)	I^{norm}_{cal} (mol^{-1})
1	2.3588	2.75	5.20	✓	1	9.4684	15.582	30.026
				✓	2	9.5078	15.444	29.637
				✓	3	9.4625	15.496	29.880
				✓	4	9.6582	15.411	29.113
2	3.1559	2.50	4.95	✓	5	9.4079	20.959	30.381
3	6.9464	2.00	4.45	✓	6	9.3408	45.549	30.211
4	9.0791	3.00	3.45	✗	7	10.700	60.813	26.941
				✗	8	10.603	60.756	27.162
				✗	9	10.694	60.772	26.937

Table 3. Integrated experimental ^{19}F NMR signal intensities of TFA for a series of trials for a set of angiotensin II (analyte) samples.

Sample #	m_{ana} (mg)	h_b (mm)	h_t (mm)	quant. volume	Trial #	I^E_{ana} (10^9)	I_{ana} (10^9)	I^{norm}_{ana} (mol^{-1})
1	3.7918	2.50	4.95	✓	1	9.4107	6.8382	7.2836
2	4.4113	2.00	4.45	✓	2	9.5711	8.0746	7.2689
3	4.9675	3.00	3.45	✗	3	10.771	8.4096	5.9737
				✗	4	10.784	8.3594	5.9311
				✗	5	10.847	8.7656	6.1831
4	5.1546	2.00	4.45	✓	6	9.5193	9.6158	7.4483
5	5.7294	2.00	4.45	✓	7	9.5883	10.727	7.4219
6	6.2626	2.00	4.45	✓	8	9.4745	11.612	7.4381

normalized integrated signal intensity per mol and per nucleus of the calibrant. The definition of I^{norm}_{ana} and I^{norm}_{cal} is very useful, as it allows for determining them independently for a series of NMR experiments of the calibrant and analyte, respectively. As we will see below, the final mass fraction w_{cal} of the calibrant may then easily be determined using non-parametric bootstrap re-sampling [76, 77] of both I^{norm}_{ana} and I^{norm}_{cal} to determine the mean and extended uncertainty of w_{cal}.

Tables 2 and 3 show the results of a series of ^{19}F solid-state NMR measurements of the calibrant BTFMBA and the analyte TFA in angiotensin II, respectively. In each case it is indicated whether or not the sample was located inside the quantitative volume of the rotor. The raw integrated intensities of the NMR resonance lines and the ERETIC signal are listed next to the normalized molar signal intensities I^{norm}_{ana} and I^{norm}_{cal}, respectively.

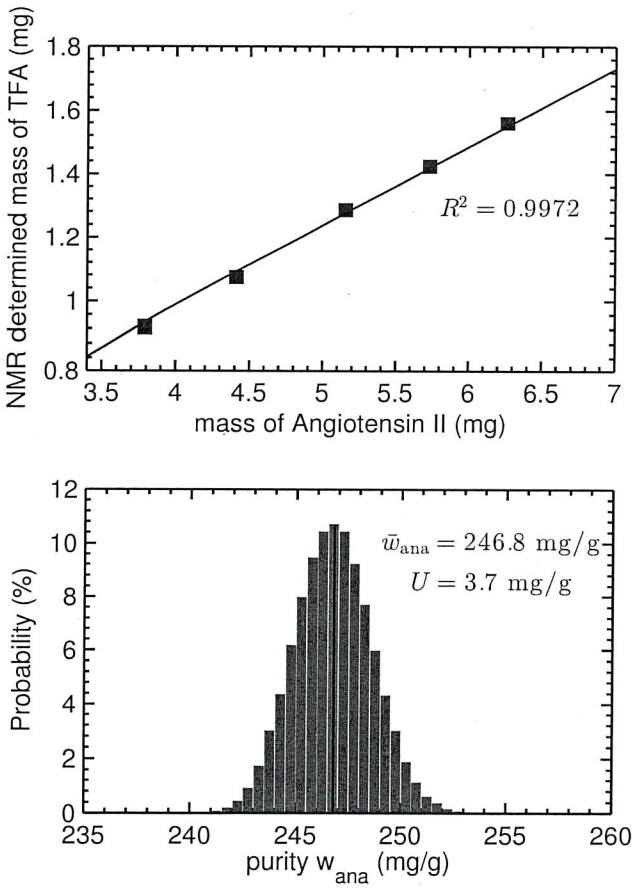

Figure 5. Top: NMR determined mass of TFA in angiotensin II as a function of the gravimetrically determined sample mass of angiotensin II. Bottom: Histogram of the TFA mass fraction (purity) w_{ana} calculated using bootstrap re-sampled values of the normalized molar signal intensities.

The mass of TFA determined by ^{19}F solid-state NMR as function of the gravimetrically determined angiotensin II sample mass is plotted in the top of figure 5. We obtain a linear relationship with $R^2 = 0.9972$. In order to obtain the mass fraction w_{ana} of TFA together with the expanded uncertainty, we performed non-parametric bootstrap re-sampling with replacement [76, 77] of the normalized molar signal intensities $I_{\text{ana}}^{\text{norm}}$ and $I_{\text{cal}}^{\text{norm}}$ obtained using the quantitative volume of the rotor. In the case of angtiotensin II the 5 values obtained for $I_{\text{ana}}^{\text{norm}}$ were re-sampled, whereas in case of BTFMBA the 6 values obtained for $I_{\text{cal}}^{\text{norm}}$ were re-sampled. For each case the means $\bar{I}_{\text{ana}}^{\text{norm}}$ and $\bar{I}_{\text{cal}}^{\text{norm}}$ were calculated. The histogram of the mass fraction $w_{\text{ana}} = \bar{I}_{\text{ana}}^{\text{norm}} / \bar{I}_{\text{cal}}^{\text{norm}}$ calculated as the ratio of the means is shown in the bottom of figure 5. From this distribution we determine the average

mean TFA mass fraction to be $\bar{w}_{\text{ana}} = 246.8$ mg/g with and extended uncertainty of $U = 3.7$ mg/g. This value is in excellent agreement with the TFA mass fraction of 248.3 mg/g ($U = 2.3$ mg/g) in a sample of ANGII-1 determined recently by ^{19}F-qNMR in solution using BTFMBA as internal calibrant [3].

From the calibration curve in the top of figure 5 the limit of detection for TFA in ANGII-1, LOD $= 3.3\sigma/S$, and the limit of quantification, LOD $= 10\sigma/S$, can be determined, where σ and S are the standard error and the slope of the regression line, respectively, [78]. We obtain values of LOD = 162 μg and LOQ = 491 μg for the mass of ANGII-1, respectively, for the case of 2048 co-added ^{19}F NMR transients. Note that these values are significant larger than the ones that would be obtained if estimating the mass required to achieve a signal to noise ratio in the NMR spectrum of 3 and 10 for the LOD and LOQ, respectively. The main reason is that the calibration curve in figure 5 is affected by insufficiencies in the ^{19}F background suppression and baseline correction, whereas a simple determination of the signal to noise ratio is not. Hence, a calibration curve is much more accurate to estimate the LOD and LOQ for solid-state ^{19}F-qNMR.

4. Conclusions

We presented a thorough and rigorous protocol for solid-state ^{19}F-qNMR employing a certified reference material as external calibrant to provide metrological traceability to absolutely quantify the TFA content in peptide samples. The protocol includes experimentally determining the quantitative volume of the solid-state NMR rotor and the use of the ERETIC method to compensate for possible variations in the sensitivity of the rf resonance circuit under samle changes. Furthermore, the EASY method was applied to effectively suppress the ^{19}F background signals of the standard commercial solid-state NMR probehead. We successfully applied the protocol to quantify the amount of TFA in a sample of the peptide angiotensin II candidate NRC certified reference material ANGII-1. The results for the TFA mass fraction we obtained (246.8 mg/g, $U = 3.7$ mg/g) following our solid-state ^{19}F-qNMR protocol are in excellent agreement with the TFA mass fraction (248.3 mg/g, $U = 2.3$ mg/g) obtained with ^{19}F-qNMR in solution employing an internal calibrant. The solid-state ^{19}F-qNMR protocol is applicable in all applications that require non-destructive metrological traceable quantification of fluorine sample contents, such as quantification of surface functional groups [66, 67]

Acknowledgments

The authors would like to thank Samuel Camiré for machining the inserts and Don Leek, Juris Meija and James Bennett for discussions and experimental help. M. R. was supported

by the NRC co-op program.

References

[1] Vitzthum F, Siest G, Bunk D M, Preckel T, Wenz C, Hoerth P, Schulz-Knappe P, Tammen H, Adamkiewicz J, Merlini G and Anderson N L 2007 Metrological sharp shooting for plasma proteins and peptides: The need for reference materials for accurate measurements in clinical proteomics and in vitro diagnostics to generate reliable results *Proteomics: Clin. Appl.* **1** 1016–1035

[2] Hoofnagle A N, Whiteaker J R, Carr S A, Kuhn E, Liu T, Massoni S A, Thomas S N, Townsend R R, Zimmerman L J, Boja E, Chen J, Crimmins D L, Davies S R, Gao Y, Hiltke T R, Ketchum K A, Kinsinger C R, Mesri M, Meyer M R, Qian W J, Schoenherr R M, Scott M G, Shi T, Whiteley G R, Wrobel J A, Wu C, Ackermann B L, Aebersold R, Barnidge D R, Bunk D M, Clarke N, Fishman J B, Grant R P, Kusebauch U, Kushnir M M, Lowenthal M S, Moritz R L, Neubert H, Patterson S D, Rockwood A L, Rogers J, Singh R J, Van Eyk J E, Wong S H, Zhang S, Chan D W, Chen X, Ellis M J, Liebler D C, Rodland K D, Rodriguez H, Smith R D, Zhang Z, Zhang H and Paulovich A G 2016 Recommendations for the generation, quantification, storage, and handling of peptides used for mass spectrometry–based assays *Clin. Chem.* **62** 48–69

[3] Melanson J E, Thibeault M P, Stocks B B, Leek D M, McRae G and Meija J 2018 Purity assignment for peptide certified reference materials by combining qNMR and LC-MS/MS amino acid analysis results: application to angiotensin II *Anal. Bioanal. Chem.* **410** 6719–6731

[4] Josephs R D, Li M, Song D, Daireaux A, Choteau T, Stoppacher N, Westwood S, Wielgosz R, Xiao P, Liu Y, Gao X, Zhang C, Zhang T, Mi W, Quan C, Huang T, Li H, Melanson J E, Ün I, Gören A C, Quaglia M and Warren J 2017 Pilot study on peptide purity—synthetic human C-peptide *Metrologia* **54** 08011

[5] Josephs R D, Li M, Song D, Westwood S, Stoppacher N, Daireaux A, Choteau T, Wielgosz R, Xiao P, Liu Y, Gao X, Zhang C, Zhang T, Mi W, Quan C, Huang T, Li H, Flatschart R, Oliveira R B, Melanson J E, Ohlendorf R, Henrion A, Kinumi T, Wong L, Liu Q, Senal M O, Vatansever B, Ün I, Gören A C, Akgöz M, Quaglia M and Warren J 2017 Key comparison study on peptide purity—synthetic human C-peptide *Metrologia* **54** 08007

[6] Josephs R D, Stoppacher N, Daireaux A, Choteau T, Lippa K A, Phinney K W, Westwood S and Wielgosz R I 2018 State-of-the-art and trends for the SI traceable value assignment of the purity of peptides using the model compound angiotensin I *TrAC, Trends Anal. Chem.* **101** 108–119

[7] Stocks B B, Thibeault M P, Meija J and Melanson J E 2018 Assessing MS-based quantitation strategies for low-level impurities in peptide reference materials: application to angiotensin II *Anal. Bioanal. Chem.* **410** 6963–6972

[8] Barantin L, Pape A L and Akoka S 1997 A new method for absolute quantitation MRS metabolites *Magn. Reson. Med.* **38** 179–182

[9] Akoka S, Barantin L and Trierweiler M 1999 Concentration measurement by proton NMR using the ERETIC method *Anal. Chem.* **71** 2554–2557

[10] Akoka S and Trierweiler M 2002 Improvement of the ERETIC method by digital synthesis of the signal and addition of a broadband antenna inside the NMR probe *Instrum. Sci. Technol.* **30** 21–29

[11] Remaud G S, Silvestre V and Akoka S 2005 Traceability in quantitative NMR using an electronic signal as working standard *Accred. Qual. Assur.* **10** 415420

[12] Wider G and Dreier L 2006 Measuring protein concentrations by NMR spectroscopy *J. Am. Chem. Soc.* **128** 2571–2576

[13] Hoult D I and Richards R E 1976 The signal-to-noise ratio of the nuclear magnetic resonance experiment *J. Magn. Reson.* **24** 71–85
[14] Malz F 2008 Quantitative NMR in the solution state NMR *NMR Spectroscopy in Pharmaceutical Analysis* ed Holzgrabe U, Wawer I and Diehl B (Amsterdam: Elsevier) chap 2, pp 43–62
[15] Holzgrabe U 2010 Quantitative NMR spectroscopy in pharmaceutical applications *Prog. NMR Spectrosc.* **57** 229–240
[16] Wawer I 2008 qNMR in solid state *NMR Spectroscopy in Pharmaceutical Analysis* ed Holzgrabe U, Wawer I and Diehl B (Amsterdam: Elsevier) chap 3, pp 63–82
[17] Wawer I 2008 Solid-state measurements of drugs and drug formulations *NMR Spectroscopy in Pharmaceutical Analysis* ed Holzgrabe U, Wawer I and Diehl B (Amsterdam: Elsevier) chap 4, pp 201–231
[18] Andrew E R, Bradbury A and Eades R G 1959 Removal of dipolar broadening of nuclear magnetic resonance spectra of solids by specimen rotation *Nature* **183** 1802–1803
[19] Lowe I J 1959 Free induction decay of rotating solids *Phys. Rev. Lett.* **2** 285–287
[20] Schaefer J and Stejskal E O 1976 Carbon-13 nuclear magnetic resonance of polymers spinning at the magic angle *J. Am. Chem. Soc.* **98** 1031–1032
[21] Stejskal E O, Schaefer J and Waugh J S 1977 Magic-angle spinning and polarization transfer in proton-enhanced NMR *J. Magn. Reson.* **28** 105–112
[22] Ripmeester J A 1980 Application of solid state ^{13}C NMR to the study of polymorphs, clathrates and complexes *Chem. Phys. Lett.* **74** 536–538
[23] Harris R K, Hodgkinson P, Larsson T and Muruganantham A 2005 Quantification of bambuterol hydrochloride in a formulated product using solid-state NMR *J. Pharm. Biomed. Anal.* **38** 858–864
[24] Harris R K 2007 Applications of solid-state NMR to pharmaceutical polymorphism and related matters *J. Pharm. Pharmacol.* **59** 225–239
[25] Ziarelli F and Caldarelli S 2006 Solid-state NMR as an analytical tool: Quantitative aspects *Solid State Nucl. Magn. Reson.* **29** 214–218
[26] Ziarelli F, Viel S, Sanchez S, Cross D and Caldarelli S 2007 Precision and sensitivity optimization of quantitative measurements in solid state NMR *J. Magn. Reson.* **188** 260–266
[27] Sanchez S, Ziarelli F, Viel S, Delaurent C and Caldarelli S 2008 Improved solid-state NMR quantifications of active principles in pharmaceutical formulations *J. Pharm. Biomed. Anal.* **47** 683–687
[28] Vogt F G 2010 Evolution of solid-state NMR in pharmaceutical analysis *Future Med. Chem.* **2** 915–921
[29] Vogt F G 2015 Characterization of pharmaceutical compounds by solid-state NMR *eMagRes* **4** 255–268
[30] Gerstein B and Dybowski C 1985 *Transient techniques in NMR of solids: An introduction to theory and practice* (United States: Academic Press Inc)
[31] Zhang S, Wu X and Mehring M 1990 Successive polarization under mismatched Hartmann-Hahn condition *Chem. Phys. Lett.* **166** 92–94
[32] Jeschke G and Grossmann G 1993 Spinning-sideband-pattern deviations in cross-polarization MAS NMR spectra *J. Magn. Reson. A* **103** 323–328
[33] Nevzorov A A 2011 Ergodicity and efficiency of cross-polarization in NMR of static solids *J. Magn. Reson.* **209** 161–166
[34] Raya J, Perrone B and Hirschinger J 2013 Chemical shift powder spectra enhanced by multiple-contact cross-polarization under slow magic-angle spinning *J. Magn. Reson.* **227** 93–102
[35] Johnson R L and Schmidt-Rohr K 2014 Quantitative solid-state ^{13}C NMR with signal enhancement by multiple cross polarization *J. Magn. Reson.* **239** 44–49

[36] Saïdi F, Taulelle F and Martineau C 2016 Quantitative ^{13}C solid-state NMR spectra by multiple-contact cross-polarization for drug delivery: From active principles to excipients and drug carriers *J. Pharm. Sci.* **105** 2397–2401

[37] Atalla R H, Gast J C, Sindorf D W, Bartuska V J and Maciel G E 1980 ^{13}C NMR spectra of cellulose polymorphs *J. Am. Chem. Soc.* **102** 3249–3251

[38] Earl W L and VanderHart D L 1980 High resolution, magic angle sampling spinning ^{13}C NMR of solid cellulose I *J. Am. Chem. Soc.* **102** 3251–3252

[39] Atalla R H and VanderHart D L 1984 Native cellulose: A composite of two distinct crystalline forms *Science* **223** 283–285

[40] VanderHart D L and Atalla R H 1984 Studies of microstructure in native celluloses using solid-state ^{13}C NMR *Macromolecules* **17** 1465–1472

[41] Lennholm H, Larsson T and Iversen T 1994 Determination of cellulose I_α and I_β in lignocellulosic materials *Carbohyd. Res.* **261** 119–131

[42] Wormald P, Wickholm K, Larsson P T and Iversen T 1996 Conversions between ordered and disordered cellulose. effects of mechanical treatment followed by cyclic wetting and drying *Cellulose* **3** 141–152

[43] Newman R H and Hemmingson J A 1995 Carbon-13 Nmr distinction between categories of molecular order and disorder in cellulose *Cellulose* **2** 95–110

[44] Newman R H 1998 Evidence for assignment of ^{13}C signals to cellulose crystallite surfaces in wood, pulp and isolated celluloses *Holzforschung* **52** 157–159

[45] Newman R H 1999 Estimation of the lateral dimensions of cellulose crystallites using NMR signal strengths *Solid State Nucl. Magn. Reson.* **15** 21–29

[46] Larsson P T, Wickholm K and Iversen T 1997 A CP/MAS ^{13}C NMR investigation of molecular ordering in celluloses *Carbohyd. Res.* **302** 19–25

[47] Wickholm K, Larsson P T and Iversen T 1998 Assignment of non-crystalline forms in cellulose I by CP/MAS ^{13}C NMR spectroscopy *Carbohyd. Res.* **312** 123–129

[48] Atalla R H and VanderHart D L 1999 The role of solid state ^{13}C NMR spectroscopy in studies of the nature of native celluloses *Solid State Nucl. Magn. Reson.* **15** 1–19

[49] Chunilall V, Bush T, Larsson P T, Iversen T and Kindness A 2010 A CP/MAS ^{13}C-NMR study of cellulose fibril aggregation in eucalyptus dissolving pulps during drying and the correlation between aggregate dimensions and chemical reactivity *Holzforschung* **64** 693–698

[50] Pan J, Hamad W and Straus S K 2010 Parameters affecting the chiral nematic phase of nanocrystalline cellulose films *Macromolecules* **43** 3851–3858

[51] Park S, Johnson D K, Ishizawa C I, Parilla P A and Davis M F 2009 Measuring the crystallinity index of cellulose by solid state ^{13}C nuclear magnetic resonance *Cellulose* **16** 641–647

[52] Park S, Baker J O, Himmel M E, Parilla P A and Johnson D K 2010 Cellulose crystallinity index: Measurement techniques and their impact on interpreting cellulase performance *Biotechnol. Biofuels* **3** 10

[53] Larsson P T, Svensson A and Wågberg L 2013 A new, robust method for measuring average fibre wall pore sizes in cellulose I rich plant fibre walls *Cellulose* **20** 623–631

[54] Sacui I A, Nieuwendaal R C, Burnett D J, Stranick S J, Jorfi M, Weder C, Foster E J, Olsson R T and Gilman J W 2014 Comparison of the properties of cellulose nanocrystals and cellulose nanofibrils isolated from bacteria, tunicate, and wood processed using acid, enzymatic, mechanical, and oxidative methods *ACS Appl. Mater. Interfaces* **6** 6127–6138

[55] Bernardinelli O D, Lima M A, Rezende C A, Polikarpov I and deAzevedo E R 2015 Quantitative ^{13}C multiCP solid-state NMR as a tool for evaluation of cellulose crystallinity index measured directly inside sugarcane biomass *Biotechnol. Biofuels* **8** 110

[56] Brinkmann A, Chen M, Couillard M, Jakubek Z J, Leng T and Johnston L J 2016 Correlating cellulose nanocrystal particle size and surface area *Langmuir* **32** 6105–6114

[57] Fu L, McCallum S A, Miao J, Hart C, Tudryn G J, Zhang F and Linhardt R J 2015 Rapid and accurate determination of the lignin content of lignocellulosic biomass by solid-state NMR *Fuel* **141** 39–45

[58] King C, Stein R S, Shamshina J L and Rogers R D 2017 Measuring the purity of chitin with a clean, quantitative solid-state NMR method *ACS Sustainable Chem. Eng.* **5** 8011–8016

[59] Avadhut Y S, Schneider D and Schmedt auf der Günne J 2009 A method for improved quantification of ^{1}H NMR signals under low-resolution conditions for solids *J. Magn. Reson.* **201** 1–6

[60] Schmedt auf der Günne J, Mangstl M and Kraus F 2012 Occurrence of difluorine F_2 in nature—In situ proof and quantification by NMR spectroscopy *Angew. Chem. Int. Ed.* **51** 7847–7849

[61] Ghassemzadeh L and Holdcroft S 2013 Quantifying the structural changes of perfluorosulfonated acid ionomer upon reaction with hydroxyl radicals *J. Am. Chem. Soc.* **135** 8181–8184

[62] Fry R A, Tsomaia N, Pantano C G and Mueller K T 2003 ^{19}F MAS NMR quantification of accessible hydroxyl sites on fiberglass surfaces *J. Am. Chem. Soc.* **125** 2378–2379

[63] Budarin V L, Clark J H and Tavener S J 2004 Surface energy and surface area measurements by ^{19}F MAS NMR of adsorbed trifluoroacetic acid *Chem. Commun.* (5) 524–525

[64] Budarin V L, Clark J H, Deswarte F E I, Mueller K T and Tavener S J 2007 ^{19}F magic angle spinning NMR reporter molecules: empirical measures of surface shielding, polarisability and H-bonding *Phys. Chem. Chem. Phys.* **9**(18) 2274–2283

[65] Sanders R L, Washton N M and Mueller K T 2010 Measurement of the reactive surface area of clay minerals using solid-state nmr studies of a probe molecule *J. Phys. Chem. C* **114** 5491–5498

[66] Huber A, Behnke T, Würth C, Jaeger C and Resch-Genger U 2012 Spectroscopic characterization of coumarin-stained beads: Quantification of the number of fluorophores per particle with solid-state ^{19}F-NMR and measurement of absolute fluorescence quantum yields *Anal. Chem.* **84** 3654–3661

[67] Hennig A, Dietrich P M, Hemmann F, Thiele T, Borcherding H, Hoffmann A, Schedler U, Jäger C, Resch-Genger U and Unger W E S 2015 En route to traceable reference standards for surface group quantifications by XPS, NMR and fluorescence spectroscopy *Analyst* **140**(6) 1804–1808

[68] Jaeger C and Hemmann F 2014 EASY: A simple tool for simultaneously removing background, deadtime and acoustic ringing in quantitative NMR spectroscopy—Part I: Basic principle and applications *Solid State Nucl. Magn. Reson.* **57–58** 22–28

[69] Jaeger C and Hemmann F 2014 EASY: A simple tool for simultaneously removing background, deadtime and acoustic ringing in quantitative NMR spectroscopy. Part II: Improved ringing suppression, application to quadrupolar nuclei, cross polarisation and 2D NMR *Solid State Nucl. Magn. Reson.* **63–64** 13–19

[70] Frye J S and Maciel G E 1982 Setting the magic angle using a quadrupolar nuclide *J. Magn. Reson.* **48** 125–131

[71] Harris R K, Becker E D, Cabral de Menezes S M, Granger P, Hoffman R E and Zilm K W 2008 Further conventions for NMR shielding and chemical shifts (IUPAC recommendations 2008) *Pure Appl. Chem.* **80** 59–84

[72] Markley J L, Horsley W J and Klein M P 1971 Spinlattice relaxation measurements in slowly relaxing complex spectra *J. Chem. Phys.* **55** 3604–3605

[73] Duncan T M 1997 *Principal Components of Chemical Shift Tensors: A Compilation* 2nd ed (Madison, WI, USA: The Farragut Press)

[74] Maricq M M and Waugh J S 1979 NMR in rotating solids *J. Chem. Phys.* **70** 3300–3316

[75] Tyburn J M and Coutant J 2016 *TopSpin ERETIC 2 User Manual* Bruker Rheinstetten, Germany

URL `http://www.bruker.com`

[76] Efron B and Tibshirani R 1986 Bootstrap methods for standard errors, confidence intervals, and other measures of statistical accuracy *Statist. Sci.* **1** 54–75

[77] Efron B and Tibshirani R 1991 Statistical data analysis in the computer age *Science* **253** 390–395

[78] International Conference on Harmonisation of Technical Requirements for Pharmaceuticals for Human Use 1996 *Validation of Analytical Procedures: Text and Methodology* (*ICH Harmonised Tripartite Guideline* no Q2(R1))